Article

β-cyclodextrin Nanophotosensitizers for Redox-Sensitive Delivery of Chlorin e6

Jaewon Jo , Ji Yoon Kim , Je-Jung Yun , Young Ju Lee * , Young-IL Jeong *

Posted Date: 17 October 2023

doi: 10.20944/preprints202310.1006.v1

Keywords: β-Cyclodextrin; redox-sensitive; cancer targeting; photodynamic therapy; chlorin e6

Article

β-cyclodextrin Nanophotosensitizers for Redox-Sensitive Delivery of Chlorin e6

Jaewon Jo [1], Ji Yoon Kim [1], Je-Jung Yun [2], Young Ju Lee [1,*] and Young-IL Jeong [3,4,*]

[1] Gwangju Center, Korea Basic Science Institute, Gwangju 61186, Republic of Korea; jawon1119@kbsi.re.kr (J.J.); jykim1018@kbsi.re.kr (J.Y.K.) yjlee@kbsi.re.kr (Y.J.L.)
[2] Research Center for Environmentally Friendly Agricultural Life Sciences, Jeonnam Bioindustry Foundation, Jeonnam 58275, Republic of Korea; jjyoung4@hanmail.net
[3] Research Institute for Convergence of Biomedical Science and Technology, Pusan National University Yangsan Hospital, Gyeongnam 50612, Republic of Korea; nanomed@naver.com
[4] Tyros Biotechnology Inc., 75 Kneeland St. 14 Floors, Boston, MA 02111, USA
* Correspondence: yjlee@kbsi.re.kr (Y.J.L.); nanomed@naver.com (Y.-I.J.); Tel.: +82-10-9212-9859 (Y.-I.J.)

Abstract: The aim of this study is to prepare redox-sensitive nanophotosensitizers for targeted delivery of chlorin e6 (Ce6) against cervical cancer. For this purpose, Ce6 was conjugated with β-cyclodextrin (bCD) via disulfide bond creating nanophotosensitizers that were fabricated for redox-sensitive delivery of Ce6 against cancer cells. bCD was treated with succinic anhydride to synthesize succinylated bCD (bCDsu). After that, cystamine was attached to the carboxylic end of bCDsu (bCDsu-ss) and the amine end group of bCDsu-ss was conjugated with Ce6 (bCDsu-ss-Ce6). Chemical composition of bCDsu-ss-Ce6 was confirmed with ^{1}H and ^{13}C NMR spectra. bCDsu-ss-Ce6 nanophotosensitizers were fabricated by dialysis procedure. They formed small particles with an average particle size of 152.0±23.2 nm and they showed improved singlet oxygen (SO) generation in the aqueous solution under light irradiation and was significantly higher than that of Ce6 alone. Ce6 release rate from bCDsu-ss-Ce6 nanophotosensitizers was accelerated by addition of glutathione (GSH), indicating that bCDsu-ss-Ce6 nanophotosensitizers have redox-sensitive photosensitizer delivery capacity. bCDsu-ss-Ce6 nanophotosensitizers have low intrinsic cytotoxicity against CCD986Sk human skin fibroblast cells as well as Ce6 alone. However, bCDsu-ss-Ce6 nanophotosensitizers showed improved Ce6 uptake ratio, higher reactive oxygen species (ROS) production and phototoxicity compared to those of Ce6 alone. GSH addition resulted in higher Ce6 uptake ratio, ROS generation and phototoxicity than those of Ce6 alone, indicating that bCDsu-ss-Ce6 nanophotosensitizers have redox-sensitive biological activity in vitro against HeLa human cervical cancer cells. At tumor xenograft model using HeLa cells, bCDsu-ss-Ce6 nanophotosensitizers efficiently accumulated in the tumor rather than normal organs, i.e. fluorescence intensity in tumor tissues was significantly higher than those of other organs while Ce6 alone did not specifically target tumor tissue. These results indicated higher anticancer activity of bCDsu-ss-Ce6 nanophotosensitizers, by efficiently inhibiting growth of tumor in in vivo animal tumor xenograft study.

Keywords: β-Cyclodextrin; redox-sensitive; cancer targeting; photodynamic therapy; chlorin e6;

1. Introduction

Photodynamic therapy (PDT) is believed to be a safe option for treatment of cancer [1-3]. PDT, which is composed of light, oxygen and photosensitizers, can be specifically applied on the tumor tissue only and minimizing adverse physiological effect against normal cells or tissues because photosensitizers only activated and produced excess amount of reactive oxygen species (ROS) in the field of light irradiation eradicating abnormal cells [4,5]. However, PDT is suitable for epithelial or squamous cancer phenotypes such as cervical cancer, melanoma and oral cancers since the light penetration depth is normally limited to 15 mm of the physiological interface [6-8]. From these intrinsic properties, PDT is a suitable treatment option for cervical cancers because morphology of cervical cancer is mostly squamous cell carcinoma phenotype and then irradiated light is ease to penetrate to tumor tissues [9]. Furthermore, photosensitizers have little toxicity against normal cells or tissues in the absence of light irradiation and then side effects can be minimized while

 doi:10.20944/preprints202310.1006.v1

chemotherapeutic agents have serious side effects such as bone marrow depression, neurotoxicity, hematological toxicity, neutropenia and nephrotoxicity [9,10]. Despite of these advantages of PDT regimen, PDT with traditional photosensitizers has limitations in clinical application because some of them such as 5-aminolevulinic acid (5-ALA) have low tumor specificity, rapid clearance from human body, and low penetration depth against tissues, and then distributed throughout the whole body [11,12]. Furthermore, these problems induce light sensitive problems against patients [13]. Some photosensitizers such as chlorin e6 (Ce6) has low aqueous solubility and the drug resistance against cancer cells is also drawback for clinical application [14,15].

To solve these problems, various vehicles such as nanoparticles, polymer conjugates, proteins, polymeric micelles, nanomaterials and cyclodextrins have been studied [16-20]. Nano-dimensional carriers have various advantages such as long blood circulation, solubilization of hydrophobic drugs, active/passive targeting of tumor, avoidance of reticuloendothelial system uptake and site-specific delivery of bioactive agents [21-23]. For example, Lin et al. reported that Ce6 encapsulated poly(lactide-co-glycolide) nanoparticles show sustained drug release properties over 3 days, enhanced cellular uptake against HCT-116 cells and higher phototoxicity than that of Ce6 itself [16]. Polymeric micelles are frequently employed for site specific-delivery of bioactive agents against tumor [22]. Especially, cyclodextrin, which is cyclic oligosaccharide, is believed as an ideal candidate for solubilization of hydrophobic drugs and site-specific delivery of bioactive agents [20,24-26]. Paul et al. reported that hydroxypropyl-β-cyclodextrin increases aqueous solubility of Ce6 at pH 7 through formation of inclusion complex and then improves phototoxicity against oral squamous carcinoma cells through enhanced ROS production [20]. Li et al. also reported that polydopamine nanoparticles modified with β-cyclodextrin show excellent drug loading capacity of doxorubicin and Ce6, and then results in superior antitumor activity in vitro/in vivo [24]. Nanoplatforms including β-cyclodextrin can be passively accumulated in the tumor tissues, properly produced singlet oxygen under irradiation and then initiated antitumor immune responses against metastasis of breast cancer cells [25]. Xue et al. reported that β-cyclodextrin-substituted aza-boron-dipyrromethene-based photosensitizers are suitable carriers for site-specific targeting of cancer cells [26].

In this study, we synthesized succinylated β-cyclodextrin conjugated with Ce6 via disulfide linkage (bCDsu-ss-Ce6). Redox potentials are elevated in the tumor tissue and then the level of glutathione (GSH), which is key molecules for degradation of disulfide bond, is also elevated in the tumor tissues [27]. bCDsu-ss-Ce6 conjugates may have sensitivity against intracellular GSH level in cancer cells and then disintegrated intracellularly. Physicochemical and biological properties of bCDssCe6 were investigated in vitro and in vivo.

2. Results

2.1. Synthesis of bCDsu-ss-Ce6 Conjugates

Synthesis scheme of bCDsu-ss-Ce6 is showed in Figure 1. The carboxylic acid derivatives of bCD were synthesized by conjugation with succinyl anhydride (bCDsu). After that, cystamine was attached to the one end of carboxylic acid to make bCDsu-ss. Finally, Ce6 activated with EDC/NHS system was conjugated with bCDsu-ss to obtain bCDsu-ss-Ce6. Unreacted substances were removed by the dialysis procedure. To confirm each chemical structure of b-CDsu, b-CDsu-ss, bCDsu-ss-Ce6, spectroscopic methods such as NMR, Mass and IR were employed.

Ce6 has been assigned by the ^{1}H and ^{13}C NMR spectrum as shown in Figure S1. Figure S2(a) and (b) showed ^{1}H and ^{13}C NMR spectra of bCDsu obtained in D_2O due to high aqueous solubility via succinyl substitution. Directly substituted carbon(C_6) and neighboring carbon(C_5) were shifted 3.96 ppm downfield, and 1.96 ppm upfield relative to their unsubstituted counterparts (C_6', C_5'), respectively. Also, protons (H_{6a}, H_{6b}) attached to directly substituted carbon were shifted downfield by 0.4 ~ 0.62 ppm, while proton(H_5) on neighboring carbons were shifted downfield 0.18 ppm. ^{13}C NMR spectra of bCDsu indicated that specific carboxylic acid peaks of bCDsu was observed at 170 ~ 180 ppm. The degree of substitution (DS) of succinyl group could be calculated by comparing the substituted methylene peaks (H_{6a}, H_{6b}, 2H) to the anomeric proton (H_1, 1H), resulting in 6.69.

 doi:10.20944/preprints202310.1006.v1

Furthermore, the $[M+H]^+$ ion peaks of bCDsu with DS 6 and 7 were observed at *m*/*z* 1735.436 and 1835.447, respectively, in the ESI-MS analysis, as depicted in Figure S3(a and b).

bCDsu-ss was analyzed by 1D and 2D NMR spectrum as shown in Figure S4 and S5. ^1H and ^{13}C NMR spectra in Figure S4(a) and (b), respectively. ^1H-^{13}C HSQC and ^1H-^{13}C HMBC) in Figure S5(a) and (b), respectively. Carbons (C_8, C_9, C_{10}) of succinyl group conjugated with cystamine were differentiated from succinyl carbons ($C_{8'}$, $C_{9'}$, $C_{10'}$) without cystamine at around 30 ppm and 172 ppm. The degree of substitution (DS) of cystamine group could be calculated by comparing the substituted methylene peaks (H_{12}, H_{13}, 4H) to the anomeric proton (H_1, 7H), resulting in 1.25. Evidently, correlation peak between carbonyl carbon(C_{10}) of succinyl group and methylene protons(H_{11}) of cystamine in HMBC spectrum indicated clear conjugation via peptide bond. And ESI-MS spectrum shows $[M+H]^+$ peak at *m*/*z* 1969.520 in Figure S3(c).

Finally, bCDsu-ss-Ce6 was confirmed through 1D & 2D NMR and IR spectrum. As shown in Figure 2A, the ^1H Spectrum reveals a shift of H_{15a} (5.39ppm) in Ce6 to H_{15a} (5.53ppm) in bCDsu-ss-Ce6. Figure 2B(a) and (c) shows intrinsic peaks of bCDsu-ss and Ce6 in ^1H NMR spectra. As shown in Figure 2B(c), methylene proton (H_{15a}, 5.39 ppm in Figure 2B(b)) peak of Ce6 was shifted to 5.53 ppm. In ^{13}C NMR spectrum of Figure S6, most peaks were assigned except for one carbon(C_{33}), despite their weak and obscure nature. These peaks can be assigned through the projection of the correlation peaks in HSQC and HMBC. Figure S7(a) and (b) shows HSQC and HMBC of Ce6, respectively. Figure S7 (c) and (d) shows HSQC and HMBC of bCDsu-ss-Ce6 conjugates. In the HMBC spectra of Ce6 (Figure S7(b)) and bCDsu-ss-Ce6(Figure S7(d)), significant correlations were observed. In the case of Ce6, the methylene proton (H_{15a}, 5.39 ppm) peak showed correlations with α and β position carbons (C_{14}, C_{15}, C_{15b}, C_{16}) through two- and three-bond couplings. Similarly, in the HMBC spectrum of bCDsu-ss-Ce6, the formation of an amide bond between Ce6 and cystamine resulted in correlation peaks between the proton (H_{15a}, 5.53 ppm) and carbons (C_{15}, C_{34}, C_{16}), providing evidence for the successful synthesis of b-CDsu-ss-Ce6 conjugates. In the FT-IR spectrum of Figure S8, C=O stretching of amide group of bCDsu-ss-Ce6 conjugates was observed at 1650 cm^{-1}. We couldn't obtain MS spectrum of b-CDsu-ss-Ce6 conjugates due to their low solubility and ionization. Figure S8 shows the FT-IR spectra of the bCD, bCDsu, bCDsu-ss, Ce6 and bCDsu-ss-Ce6 conjugates. As shown in Figure S8, intrinsic spectrum of bCD and Ce6 was obtained, respectively. When bCD was reacted with succinic anhydride to produce bCDsu, C=O stretching of carboxylic acid group was observed at 1720~1740 cm^{-1}. When cystamine was attached to bCDsu to produce bCDsu-ss, C=O stretching of amide group was observed at around 1650 cm^{-1}. As shown in Figure 8, C=O stretching of amide group of bCDsu-ss-Ce6 conjugates was also observed at 1650 cm^{-1}. These results indicated that bCDsu, bCDsu—ss and bCDsu-ss-Ce6 conjugates was successfully synthesized.

Preprints (www.preprints.org) | NOT PEER-REVIEWED | Posted: 17 October 2023 doi:10.20944/preprints202310.1006.v1

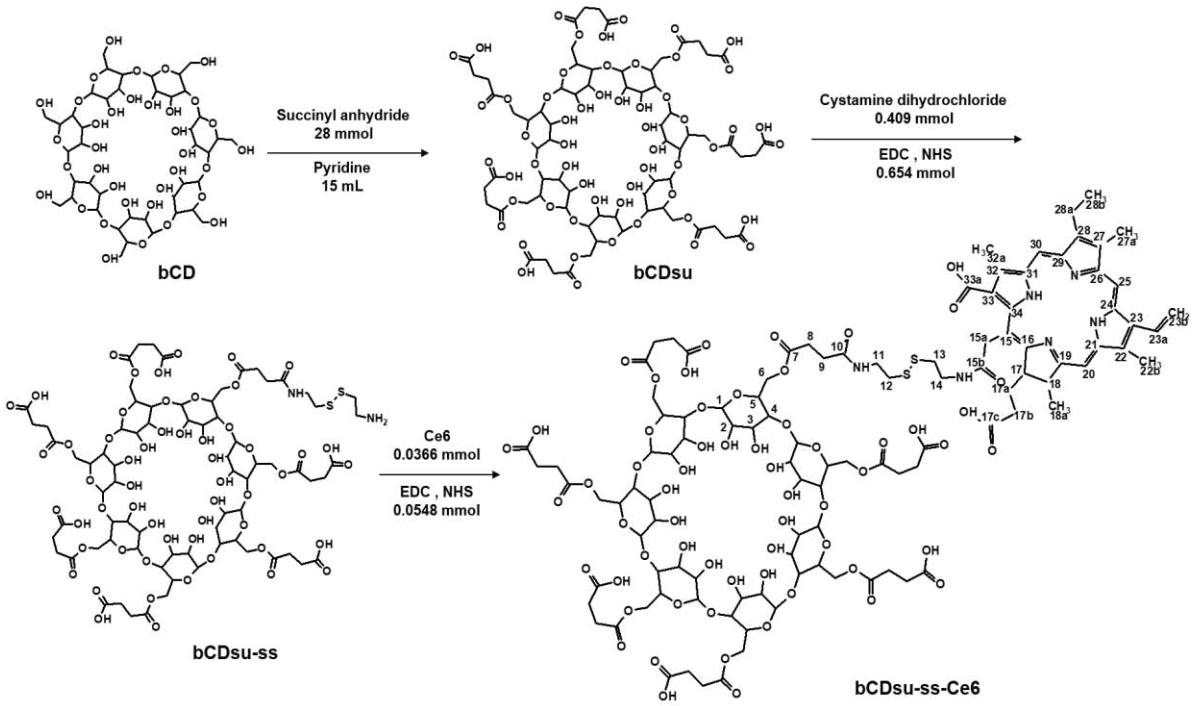

Figure 1. Synthesis scheme of bCDsu-ss-Ce6 conjugates.

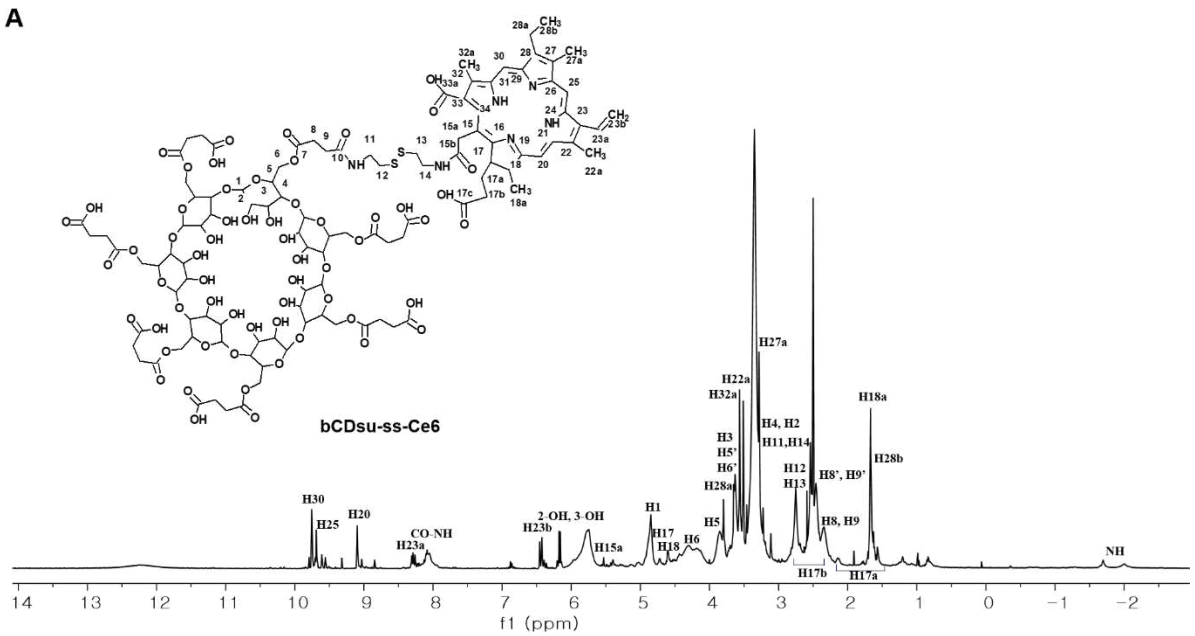

Preprints (www.preprints.org) | NOT PEER-REVIEWED | Posted: 17 October 2023 doi:10.20944/preprints202310.1006.v1

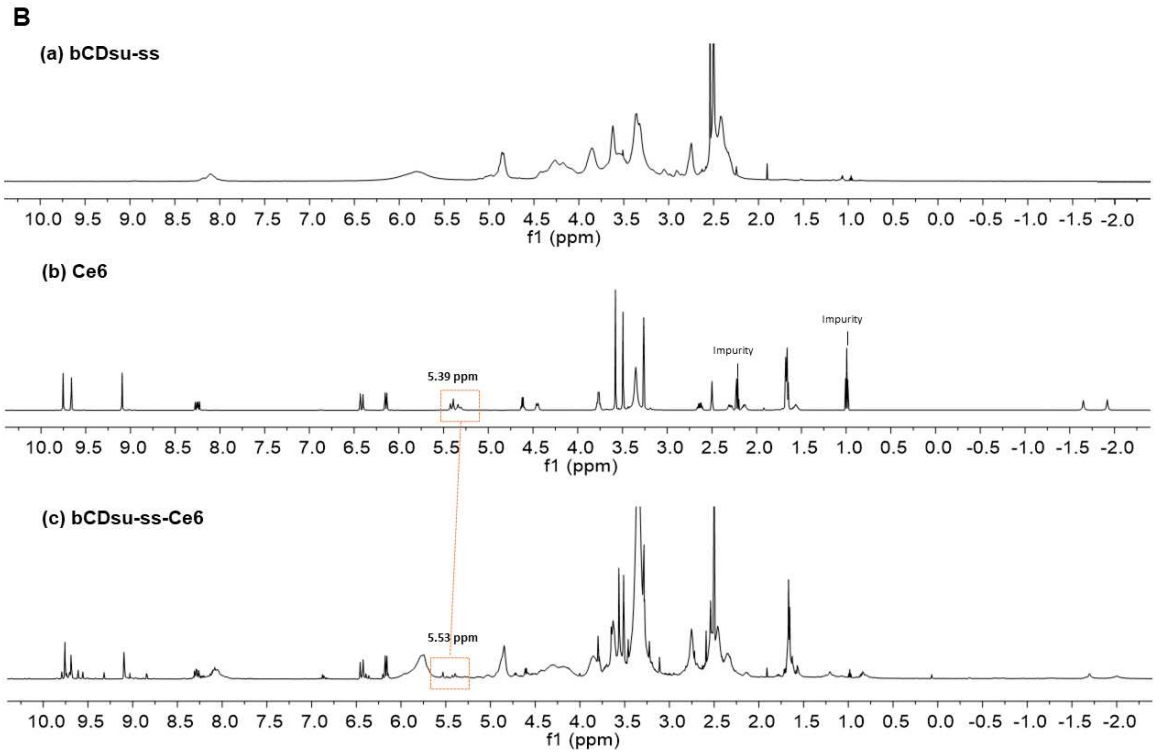

Figure 2. A. ^{1}H NMR spectrum assignment of bCDsu-ss-Ce6 conjugates. B. ^{1}H NMR spectra of (a) bCDsu-ss, (b) Ce6, (c) bCDsu-ss-Ce6.

2.2. Characterization of bCDsu-ss-Ce6 Nanophotosensitizers

Nanophotosensitizers of bCDsu-ss-Ce6 conjugates were fabricated by dialysis method. Since Ce6 is a hydrophobic molecule, hydrophobic interaction between Ce6 in the conjugates is a driving force to form self-aggregates and then they formed nanoparticles as shown in Figure 3(a), i.e. TEM images of bCDsu-ss-Ce6 nanophotosensitizers shows spherical morphology and small particle size. Their particle size distribution and zeta potential were shown in Figure 3(b) and (c). As shown in Figure 3(b), bCDsu-ss-Ce6 nanophotosensitizers showed narrow size distribution. Zeta potential of bCDsu-ss-Ce6 nanophotosensitizers also showed narrow size distribution as shown in Figure 3(c).

Table 1 summarized the characteristics of bCDsu-ss-Ce6 nanophotosensitizers. As shown in Table 1, experimental Ce6 contents in bCDsu-ss-Ce6 nanophotosensitizers were not significantly different compared to theoretical value of Ce6 contents, indicating that Ce6 contents were identical to the characterization from NMR spectra. Particle size and zeta potential of bCDsu-ss-Ce6 nanophotosensitizers was abbreviated in Table 1. Particle size was 162.9±24.4 nm as an intensity average. Polydispersity and zeta potential were 0.202 and -10.4 mV.

Preprints (www.preprints.org) | NOT PEER-REVIEWED | Posted: 17 October 2023 doi:10.20944/preprints202310.1006.v1

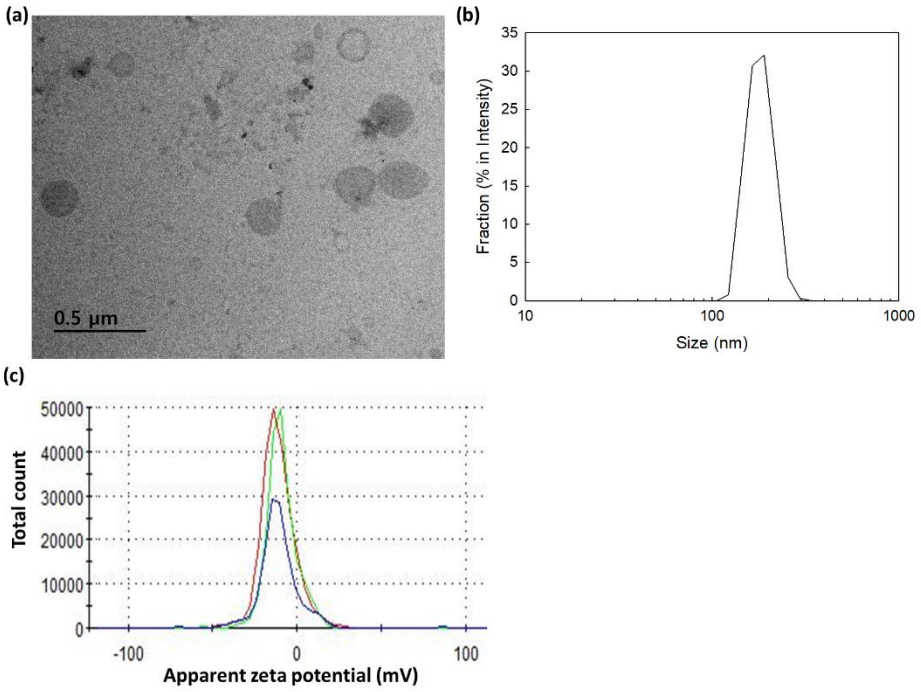

Figure 3. Characterization of bCDsu-ss-Ce6 nanophotosensitizers. (**a**) TEM photograph; (b) Typical particle size distribution; (c) zeta potential.

Table 1. Characterization of bCDsu-ss-Ce6 nanophotosensitizers.

Ce6 contents (%, w/w) [a]		Particle size distribution (nm)			Polydispersity	Zeta potential (mV)
NMR	UV	Int. ave.	Vol. ave.	Num. ave.		
17.23	17.3	162.9±24.4	152.0±23.2	142.7±20.2	0.202	-10.4

[a] Experimental drug contents were calculated from measurements of NMR and UV spectrophotometer. Drug contents = [(Ce6 weight/nanophotosensitizer weight) × 100.

Figure 4 shows the changes of fluorescence intensity of bCDsu-ss-Ce6 nanophotosensitizers according to the GSH concentration and Ce6 release properties in vitro. As shown in Figure 4(a), the fluorescence intensity of bCDsu-ss-Ce6 nanophotosensitizers was gradually increased according to the concentration of GSH, indicating that disulfide bond can be disintegrated and then Ce6 was liberated from the nanophotosensitizers. As shown in Figure 4(b), GSH addition accelerated the release rate of Ce6 from nanophotosensitizers while Ce6 release was minimized in the absence of GSH, indicating that bCDsu-ss-Ce6 nanophotosensitizers revealed redox-sensitive Ce6 release behavior in the biological system.

Preprints (www.preprints.org) | NOT PEER-REVIEWED | Posted: 17 October 2023 doi:10.20944/preprints202310.1006.v1

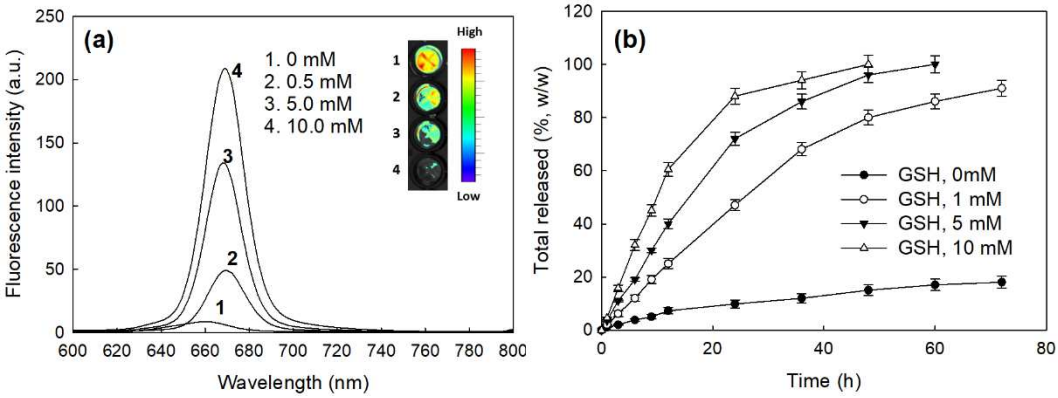

Figure 4. (a) The effect of GSH addition on the changes of fluorescence intensity of bCDsu-ss-Ce6 nanophotosensitizers. (b) The effect of GSH addition on the changes of Ce6 release from bCDsu-ss-Ce6 nanophotosensitizers.

2.3. In Vitro Cell Culture Study

Figure 5 shows the intrinsic cytotoxicity Ce6 alone, bCDsu-ss and bCDsu-ss-Ce6 nanophotosensitizers against CCD986Sk cells. All of them were not significantly cytotoxic to CCD986Sk cells, i.e. the viability of cells was higher than 80 % until 5 μg Ce6/mL of bCDsu-ss-Ce6 nanophotosensitizers and 50 μg/mL of bCDsu-ss, while Ce6 alone showed that cell viability was less than 80 % at 5 μg Ce6/mL. These results indicated that bCDsu-ss and bCDsu-ss-Ce6 nanophotosensitizers have no intrinsic cytotoxicity against normal cells.

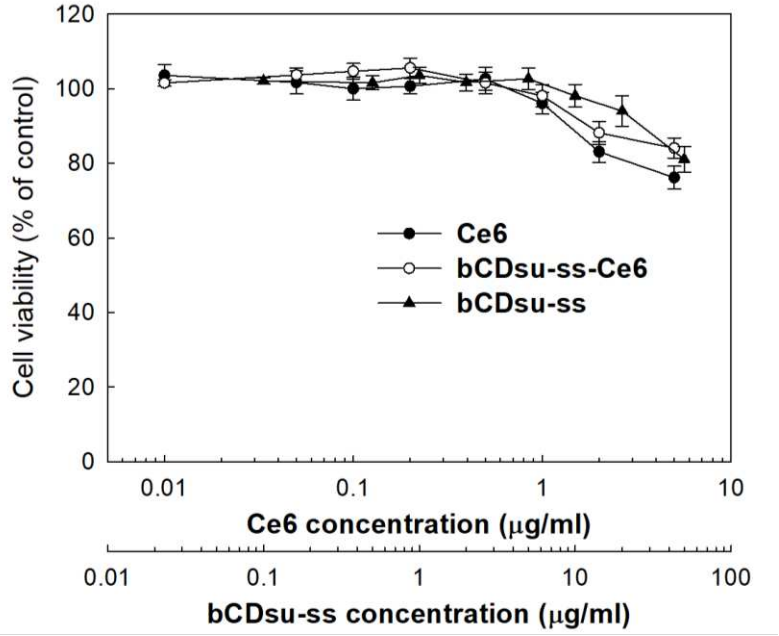

Figure 5. Intrinsic cytotoxicity of Ce6 alone, bCDsu-ss and bCDsu-ss-Ce6 nanophotosensitizers against CCD986Sk cells. CCD986Sk cells were exposed to Ce6 or nanophotosensitizers in the dark condition.

Figure 6 shows the Ce6 uptake ratio, ROS generation and phototoxicity of Ce6 alone or bCDsu-ss-Ce6 nanophotosensitizers against HeLa cells. As shown in Figure 6(a), Ce6 uptake ratio against HeLa cells were significantly higher in the treatment of bCDsu-ss-Ce6 nanophotosensitizers than that of Ce6 alone, indicating that bCDsu-ss-Ce6 nanophotosensitizers have higher potential in cellular uptake compared to Ce6. As shown in Figure 6(b), ROS generation was gradually increased according to the Ce6 concentration both of Ce6 alone and bCDsu-ss-Ce6 nanophotosensitizers. Especially, ROS

Preprints (www.preprints.org) | NOT PEER-REVIEWED | Posted: 17 October 2023 doi:10.20944/preprints202310.1006.v1

generation of bCDsu-ss-Ce6 nanophotosensitizers was 2 times higher than that of Ce6 alone, indicating that bCDsu-ss-Ce6 nanophotosensitizers have superior efficacy in ROS generation. Figure 6(c) showed the phototoxicity of Ce6 alone and bCDsu-ss-Ce6 nanophotosensitizers in the presence or absence of light irradiation. As shown in Figure 6(c), viability of light irradiation did not significantly affect the viability of HeLa cells, i.e. viability of HeLa cells was higher than 80 % until 2 μg Ce6/mL of Ce6 alone and bCDsu-ss-Ce6 nanophotosensitizers in the absence of light irradiation. When light was irradiated to the cells, cell viability was gradually decreased according to the Ce6 concentration. Especially, phototoxicity of bCDsu-ss-Ce6 nanophotosensitizers was superior than that of Ce6 alone, i.e. cell viability at 5 μg Ce6/mL was lower than 20 % of bCDsu-ss-Ce6 nanophotosensitizers while treatment of Ce6 alone revealed higher than 50 % at same concentration. These results indicated that bCDsu-ss-Ce6 nanophotosensitizers have higher efficacy in the generation of ROS and phototoxicity against cancer cells. As summarized in Table 2, IC_{50} value of bCDsu-ss-Ce6 nanophotosensitizers with light irradiation were lower than that of Ce6 alone, i.e. IC_{50} value of bCDsu-ss-Ce6 nanophotosensitizers was 1.05 mg/L while IC_{50} value of Ce6 was higher than 5 mg/L.

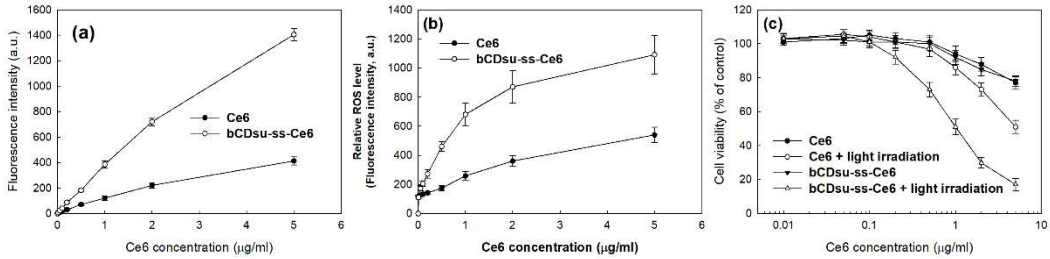

Figure 6. (a) Ce6 uptake ratio of Ce6 alone or bCDsu-ss-Ce6 nanophotosensitizers. (b) ROS generation of Ce6 alone or bCDsu-ss-Ce6 nanophotosensitizers under light irradiation. (b) PDT efficacy of Ce6 alone or bCDsu-ss-Ce6 nanophotosensitizers against HeLa cells in the absence or presence of light irradiation.

Table 2. IC_{50} of Ce6 and bCDsu-ss-Ce6 nanophotosensitizers against HeLa cells.

	IC_{50} (mg/L) [1]
Ce6	n.d. [2]
Ce6 + light irradiation	5.16
bCDsu-ss-Ce6 NP	n.d.
bCDsu-ss-Ce6 NP + light irradiation	1.05

[1] IC_{50} values were estimated from Figure 9(b). [1] n.d. = not determined.

Figure 7 shows the effect of GSH on the Ce6 uptake ratio, ROS generation and phototoxicity of Ce6 alone or bCDsu-ss-Ce6 nanophotosensitizers against HeLa cells. As shown in Figure 7(a) and (d), higher GSH concentration induced higher Ce6 uptake into the cells. As shown in Figure 7(d), GSH addition after treatment with bCDsu-ss-Ce6 nanophotosensitizers increased fluorescence intensity of HeLa cells, while GSH addition did not affect the fluorescence intensity upon treatment of Ce6 alone. Furthermore, ROS generation also increased according to the increase of GSH concentration as shown in Figure 7(b). As expected, phototoxicity also increased according to the increase of GSH concentration as shown in Figure 7(c). Furthermore, relative ROS level in the absence of GSH of nanophotosensitizers also higher than that of Ce6 itself (Figure 7(b)). These results indicated that bCDsu-ss-Ce6 nanophotosensitizers have redox-sensitivity in vitro. As shown in Figure 8, flow cytometric analysis also supported these results, i.e. peaks in flow cytometric analysis of bCDsu-ss-Ce6 nanophotosensitizers were increased compared to Ce6 alone as shown in Figure 8(a) and (b). Furthermore, peaks treated with bCDsu-ss-Ce6 nanophotosensitizers were increased by addition of GSH while Ce6 alone did not significantly change the peaks.

Preprints (www.preprints.org) | NOT PEER-REVIEWED | Posted: 17 October 2023 doi:10.20944/preprints202310.1006.v1

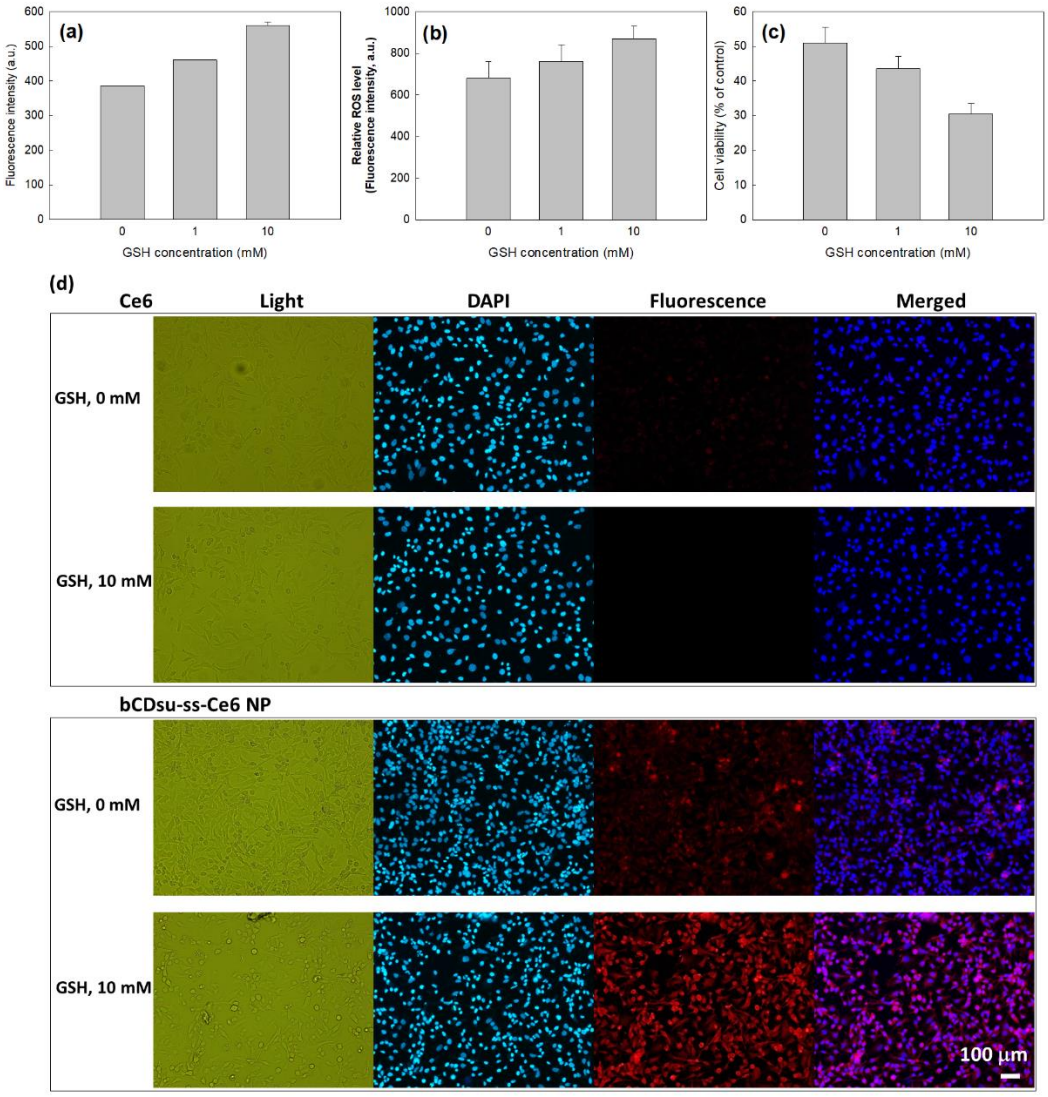

Figure 7. The effect of GSH addition on the HeLa cell culture. (a) Ce6 uptake ratio; (b) ROS generation; (c) Phototoxicity bCDsu-ss-Ce6 nanophotosensitizers under light irradiation. (d) The effect of GSH addition on the intracellular uptake of Ce6 or bCDsu-ss-Ce6 nanophotosensitizers. Bar = 100 μm.

Preprints (www.preprints.org) | NOT PEER-REVIEWED | Posted: 17 October 2023 doi:10.20944/preprints202310.1006.v1

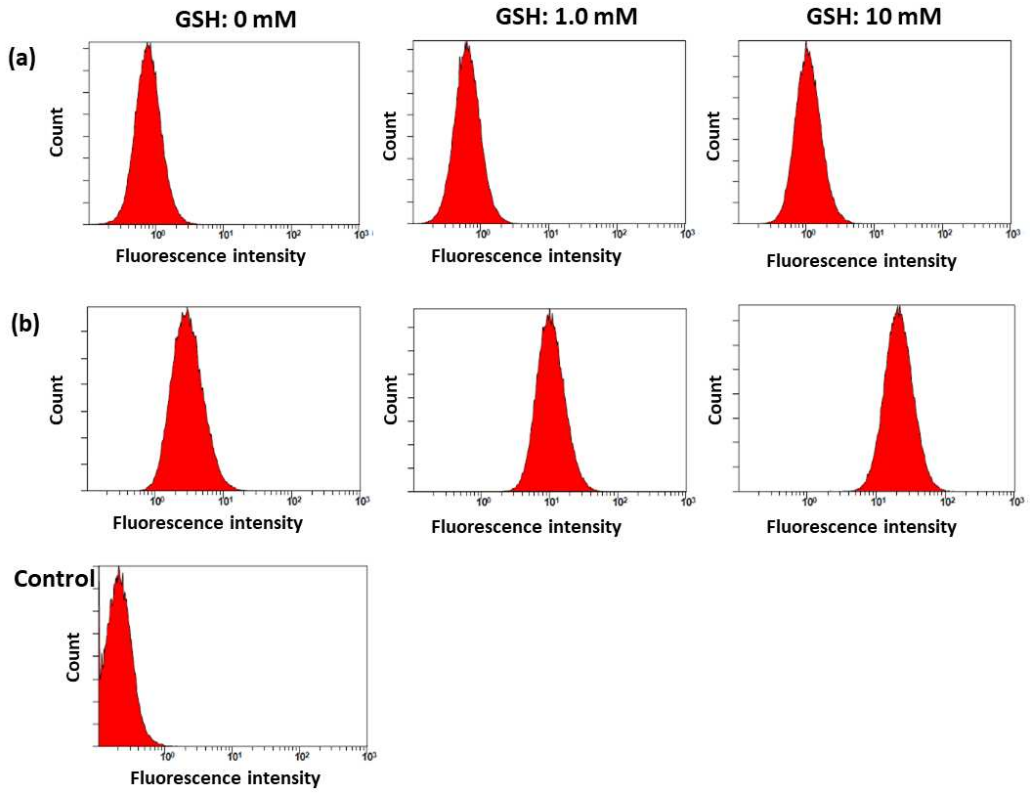

Figure 8. Flow cytometric analysis of HeLa cell culture. Cells were treated with Ce6 alone (a) and bCDsu-ss-Ce6 nanophotosensitizers (b).

2.4. In Vivo Animal Tumor Xenograft Study

Figure 9 shows the biodistribution and PDT efficacy of the nanophotosensitizers against HeLa tumor xenograft models. HeLa cells were administered to the backs of mice to make tumor xenografts for biodistribution and PDT efficacy of the nanophotosensitizers. As shown in Figure 9(a), both of Ce6 and bCDsu-ss-Ce6 nanophotosensitizers properly targeted and imaged tumor mass in the whole body and each organ images. However, relative fluorescence intensity of the tumor mass was significantly higher than that of liver in the nanophotosensitizer treatment while the changes of fluorescence intensity was not significantly changed at Ce6 treatment. These results indicated that bCDsu-ss-Ce6 nanophotosensitizers have superior potential for targeting of tumors. Figure 10(b) shows the PDT efficacy of Ce6 and bCDsu-ss-Ce6 nanophotosensitizers against HeLa tumor xenograft. As shown in Figure 9(b), the growth of tumor mass was inhibited both of Ce6 and bCDsu-ss-Ce6 nanophotosensitizer treatment under light irradiation. Especially, tumor mass of bCDsu-ss-Ce6 nanophotosensitizer plus light irradiation was significantly smaller than those of Ce6 treatment plus light irradiation. When light irradiation was absent, the growth of tumor mass was almost similar to PBS both of Ce6 and bCDsu-ss-Ce6 nanophotosensitizers. These results indicated that bCDsu-ss-Ce6 nanophotosensitizers have superior potential in tumor targeting and PDT efficacy.

Preprints (www.preprints.org) | NOT PEER-REVIEWED | Posted: 17 October 2023 doi:10.20944/preprints202310.1006.v1

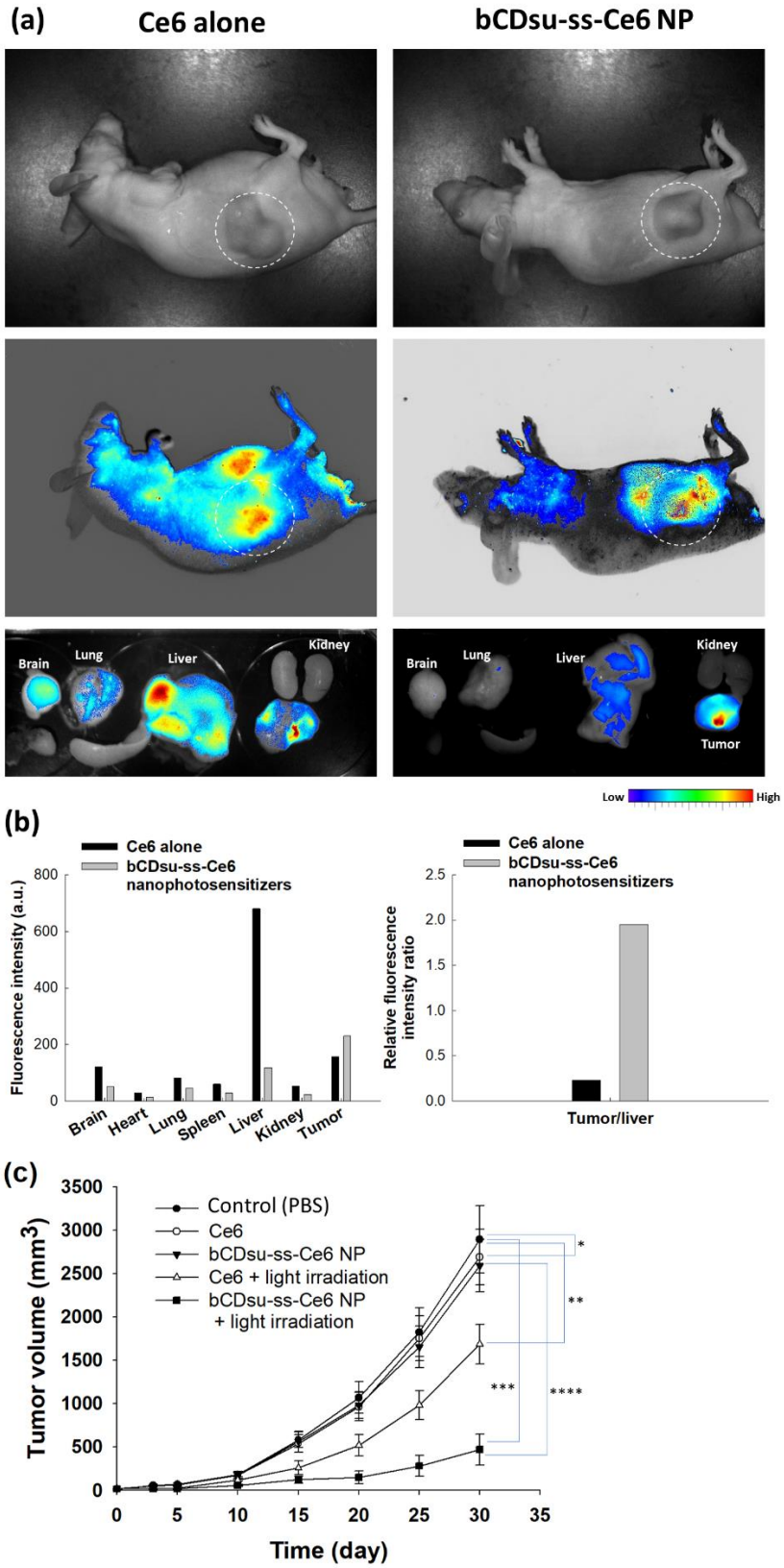

Figure 9. (a) In vivo animal imaging using a HeLa cell-bearing tumor xenograft mouse model. (b) Biodistribution of Ce6 alone or bCDsu-ss-Ce6 nanophotosensitizers (Values derived from Figure 9(a)). (c) PDT efficacy of Ce6 alone or bCDsu-ss-Ce6 nanophotosensitizers (bCDsu-ss-Ce6 nanophotosensitizers NP) with or without light irradiation on the tumor growth (Ce6 dose = 10 mg kg−1). *,**: $p < 0.01$; ***,****: $p < 0.01$.

 doi:10.20944/preprints202310.1006.v1

3. Discussion

Due to the superior properties, nano-scale carriers such as nanoparticles, polymeric micelles, polymer conjugates and nanomaterials have been extensively investigated in the field of drug targeting and stimuli-sensitive drug delivery systems [28-31]. Especially, nanoparticles having small particle sizes have been considered as an appropriate vehicle for hydrophobic anticancer agents due to their potential in site-specific delivery of bioactive agents, solubilization of lipophilic agents and ease of surface modification for recognition of specific cells [27-32]. For example, Li et al. reported that Anti-HER2 antibody-decorated poly(lactide-co-glycolide)-poly(ethylene glycol) (PLGA-PEG)/ PLGA nanoparticles can be used to target breast cancer cells and, especially, targeting efficiency can be controlled by ligand density on the nanoparticle surfaces against breast cancer cells with controlled release of docetaxel [33]. Mitchell reviewed that nanoparticles can be engineered to have adjustable particle size, stealth properties by surface modification and decoration of targeting moieties [34]. These engineered nanoparticles enable to circumvent biological barriers and to target specific cells in the diseased site. Furthermore, polymeric micelles using PEG-polyester block copolymer can be used to improve solubility of hydrophobic drugs such as coumarin 6 [35]. Supramolecular assembly based on Ce6-α-cyclodextrin with PEGylated-peptide conjugates enhances Gram-negative bacteria targeting efficiency and then eradication efficacy of bacteria film is higher than PDT with traditional photosensitizers [35].

bCDsu-ss-Ce6 conjugates formed nanoparticles having small sizes less than 200 nm as shown in Figure 3. The driving force of nanophotosensitizer formation is hydrophobic interaction between Ce6 in the bCDsu-ss-Ce6 and then associated in the aqueous solution since Ce6 is a lipophilic molecule [36,37]. Ce6 must be associated by hydrophobic interaction while bCDsu is a hydrophilic molecule and then formed nano-dimensional carriers. Cyclodextrins have been extensively used in drug delivery and pharmaceutical application [38-40]. Since they have a hydrophobic interior and hydrophilic exterior, cyclodextrins are frequently employed to form complexes with hydrophobic compounds, applied to deliver the various kind of drugs and enhanced solubility/stability of these drugs [39]. Furthermore, the inclusion complexes of cyclodextrins with hydrophobic agents are known to improve penetration efficacy into the body tissues and deliver the drugs under specific physiological conditions [41]. Paul et al. reported that inclusion complex formation between Ce6 and hydroxypropyl-β-CD (HP-β-CD) induces increase of aqueous solubility and disaggregation of Ce6 [42]. They argued that Ce6 alone shows low SO generation efficiency because Ce6 molecules are largely aggregated in the aqueous solution. These inclusion complexes improved PDT efficacy against oral squamous carcinoma cells through enhanced SO generation and phototoxicity. HP-β-CD induces disaggregation of Ce6 in the aqueous solution and then these inclusion complexes improves SO generation in the aqueous solution. Li et al. also reported that orthogonal assemblies between polydopamine-modified β-CD improved synergistic anticancer effect [43]. In our results, bCDsu-ss-Ce6 nanophotosensitizers showed higher intracellular uptake and PDT efficacy as shown in Figure 9. The mechanisms of intracellular uptake of nanophotosensitizers are practically governed by non-specific endocytosis or absorptive endocytosis because bCDsu-ss-Ce6 nanophotosensitizers have no targeting moiety on the nanoparticle surface [44]. Thakur et al also reported that lipid polymer hybrid nanoparticles encapsulating zinc-phthalocyanine and quercetin have synergistic effect in intracellular uptake and PDT against breast cancer cells [45].

Tumor microenvironment is known to have quite different physiological status compared to normal tissues, i.e. tumor microenvironment is characterized as acidic pH, enhanced permeation/retention (EPR) effect of molecules, abundant enzymes, over-expressed molecular receptors and abnormal redox potential [46-49]. Especially, abnormal redox status of tumor microenvironment is known to increase GSH level in cancer cells and then to induce drug resistant problem of anticancer agent following failure with chemotherapy [50,51]. Our results also indicated that bCDsu-ss-Ce6 nanophotosensitizers efficiently accumulates Ce6 intracellularly and generates ROS two times higher than Ce6 alone (Figure 6(a) and (b)). These results improved cancer cell death in vitro and in vivo, Figure 6(c) and Figure 9. bCDsu-ss-Ce6 nanophotosensitizers can be delivered intracellularly in HeLa cells in the higher redox status, i.e. Ce6 uptake ratio was significantly higher

 doi:10.20944/preprints202310.1006.v1

by addition of GSH and then increased ROS generation and phototoxicity as shown in Figure 7. These results must be due to the fact that Ce6 can be liberated from nanophotosensitizers in the elevated redox status as shown in Figure 6 and then our bCDsu-ss-Ce6 nanophotosensitizers have redox-sensitive potential. Otherwise, Parkhats et al. reported that quantum yield of SO production of Ce6 in aqueous solution was significantly decreased at acidic pH compared to basic pH while quantum yield of polyvinylpyrrolidone (PVP)-Ce6 conjugates at acidic pH was not significantly decreased [52]. They argued that Ce6 itself was aggregated in the acidic pH and then this phenomenon induced lower quantum yield at lower pH. However, Ce6 aggregation can be inhibited in the PVP-Ce6 conjugates and then they maintained higher quantum yield. Furthermore, Ce6 accumulation, ROS production and phototoxicity was increased according to increase of GSH concentration as shown in Figure 7. Higher GSH concentration induced stronger red fluorescence intracellular intensity as shown in Figure 7(d). These results might be due to that intracellular uptake of nanophotosensitizers is dominantly occurred, Ce6 was liberated in the intracellular GSH molecules and, after that, fluorescence intensity was increased. Also, Ce6 might be already liberated from the nanophotosensitizers in the extracellular GSH molecules and then liberated Ce6 can be entered intracellularly. Otherwise, addition of GSH was only small increase in ROS generation as shown in Figure 7(b). These results might be due to the reducing effect of GSH and then competed with ROS generation. Defensive mechanism in cancer cells may affect to the PDT efficacy and then ROS generation can be controlled by intracellular GSH level [53]. The effect of intracellular GSH level on the ROS generation and PDT effect will be discussed in the next report. bCDsu-ss-Ce6 nanophotosensitizers efficiently accumulated in tumor tissues. These phenomena also resulted in enhanced anticancer activity of bCDsu-ss-Ce6 nanophotosensitizers, suggesting that bCDsu-ss-Ce6 nanophotosensitizer as a suitable candidate for theranostic cancer treatment.

4. Materials and Methods

4.1. Materials

β-cyclodextrin (bCD), succinic anhydride, N-(3-Dimethylaminopropyl)-N′-ethylcarbodiimide hydrochloride (EDC), N-hydroxysuccinimide (NHS), cystamine dihydrochloride, triethylamine (TEA), L-glutathione (GSH), pyridine, dimethyl sulfoxide (DMSO), dimethyl sulfoxide (DMSO-D6), 2,2,2-tribromoethanol (avertin) and deuterium oxide(D_2O) were purchased from Sigma Aldrich Co. Ltd. (St. Louis, MO, USA). Chlorin e6 (Ce6) was obtained from Frontier Scientific Co. (Logan, UT, USA). All chemicals and reagents were used without further purification or treatment. The dialysis membranes having molecular weight cut-offs (MWCO) of 1000 g/mol and 2000 g/mol were obtained from Spectra/Por™ Membranes. (Rancho Dominguez, CA, USA). Avertin (2,2,2-tribromoethanol) and tert-amyl alcohol were purchased from Sigma Aldrich Chem. Co. (St. Louis, MO, USA). All experiments were performed in room temperature.

4.2. Instruments

Synthesis of bCDsu and bCDsu-ss-Ce6 was confirmed with nuclear magnetic resonance (NMR) spectroscopy [28]. Samples dissolved in D_2O or DMSO-d6 was used to analyze with NMR spectroscopy (Agilent VNMRS 600 MHz spectrometer with liquid helium cooled cryoprobe, Santa Clara, CA 95051, USA). Spectra was obtained at 25℃ and processed with MestreNova(Mnova) version 12.0.0.

Mass spectra were acquired on a quadrupole time-of-flight mass spectrometer (Xevo G2-XS, Waters, Cambridge, UK) equipped with an electrospray ionization source at Chonnam National University.

Particle size distribution was measured with a Zetasizer (Nano-ZS, Malvern, Worcestershire, UK). The effect of GSH on the particle size was performed as follows: GSH was added to aqueous solution of bCDsu-ss-Ce6 nanophotosensitizers in phosphate-buffered saline (PBS, pH 7.4, 0.01 M) and then incubated at 37 ◦C for 3 h. This solution was used to measure the particle size.

 doi:10.20944/preprints202310.1006.v1

Morphology of nanophotosensitizers was observed with transmission electron microscopy (TEM) (H7600, Hitachi Instruments Ltd., Tokyo, Japan). The one drop of aqueous solution of nanophotosensitizers was placed onto a carbon film-coated grid and then this was dried at room temperature. For negative staining, phosphotungstic acid (0.1%, w/w in H_2O) was used. TEM observation was carried out at 80 kV.

4.3. Synthesis of bCDssCe6 Conjugates

bCD was reacted with succinic anhydride to synthesize succinylated bCD (bCDsu) as reported previously [54]. Ce6 was conjugated with bCDsu via cystamine linkage bCDsu-ss-Ce6 conjugates were synthesized by conjugation of succinylated bCD with Ce6 via cystamine linkage.

Succinylated β-cyclodextrin (bCDsu): bCD (2.27 g, 2 mmol) was dissolved in 15 mL pyridine and excess quantity of succinic anhydride (2.8 g, 28 mmol) was added to the solution and stirred 16 hours at room temperature under nitrogen atmosphere. The pyridine was evaporated in a smart evaporator under vacuum at 50 °C and then was added acetone to the precipitate. The acetone mixture was filtrated and washed with acetone 2~3 times and resulting precipitate was dried overnight. Resultant products were 3.13 g and the yield was 85 % (w/w).

Cystamine-conjugated bCDsu (bCDsu-ss): bCDsu (300 mg, 0.163 mmol) dissolved in DMSO (15 mL) was mixed with 4 equivalents each of EDC (125.33 mg,0.654 mmol) and NHS (75.25 mg, 0.654 mmol). This solution was stirred for 3 hours at room temperature under nitrogen atmosphere. After that, cystamine dihydrochloride (92.02 mg, 0.409 mmol) and TEA (41.35 mg, 0.409 mmol) dissolved in DMSO (5 mL) was added dropwise into the stirred solution. The reaction mixture was magnetically stirred for 4 hours at room temperature under nitrogen atmosphere. The resulting solution was introduced into dialysis membrane (MWCO: 1000 g/mol) and then dialyzed against deionized water for 2 days. Deionized water was exchanged every 3 hours for 2 days. After that, dialyzed solution was freeze-dried for 2 days and bCDsu-ss was obtained as a white solid. Resultant products were 178 mg and the yield was 52 % (w/w).

Ce6-conjugated bCDsu-ss (bCDsu-ss-Ce6): Ce6 (21.82 mg, 0.0366 mmol) dissolved in DMSO (6 mL) was mixed with 1.5 equivalents each of EDC (10.52 mg, 0.0548 mmol) and NHS (6.312 mg, 0.0548 mmol). This solution was stirred for 4 hours at room temperature under nitrogen atmosphere. bCDsu-ss (100 mg, 0.0475 mmol) dissolved in DMSO (4 mL) was added dropwise into the stirred solution. The reaction mixture was magnetically stirred for 2 days in room temperature under nitrogen atmosphere. The resulting solution was introduced into dialysis membrane (MWCO: 1000 Da) and then dialyzed against DMSO for a few hours and then against deionized water for 2 days. Deionized water was exchanged every 3 hours. Dialyzed solution was freeze-dried for 2 days and bCDsu-ss-Ce6 was obtained as a dark solid. Resultant products were 55 mg and the yield was 59 % (w/w).

4.4. Fabrication of bCDsu-ss-Ce6 Nanophotosensitizers

bCDsu-ss-Ce6 (20 mg) was reconstituted in 2 mL of deionized water and then DMSO (3 mL) was added. This solution was poured into 10 mL deionized water and introduced into a dialysis membrane (MWCO: 2000 Da). This solution was then dialyzed against deionized water for 1 day with exchange of deionized water at 3 h intervals. The resulting solution was used for analysis or lyophilized for 2 d.

4.5. Fluorescence Spectra

Fluorescence emission spectra of nanophotosensitizers was measured with fluorescence spectrofluorophotometer (Shimadzu RF-5301PC spectrofluorophometer, Kyoto, Japan). Ce6 concentration of nanophotosensitizers was adjusted to 0.1 mg/mL PBS with or without GSH. This solution was allowed to stand for 3 h at 37 ◦C and then fluorescence emission spectra was recorded between 600 nm and 800 nm (Excitation wavelength: 400 nm). For fluorescence images were acquired

Preprints (www.preprints.org) | NOT PEER-REVIEWED | Posted: 17 October 2023 doi:10.20944/preprints202310.1006.v1

with Maestro 2 small animal imaging instrument (Cambridge Research and Instrumentation Inc., Hopkinton, MA, USA).

4.6. Drug Release Study

Nanophotosensitizers were prepared as described in 2.4. The volume of nanophotosensitizer solution was adjusted to 20 mL (1 mg/mL as bCDsu-ss-Ce6 conjugates) with deionized water. This solution (5 mL) was introduced into a dialysis membrane (MWCO: 2000 Da) and then transferred into 45 mL of PBS (pH 7.4, 0.01 M) in a conical tube. GSH was added to this solution to study the effect of GSH on the drug release properties. These solutions were incubated with shaking incubator (100 rpm) at 37 ◦C. External PBS solution was collected at predetermined time intervals to measure the liberated Ce6 and then fresh PBS was added to vials. For measurement of Ce6 concentration, collected samples were measured with a UV-VIS spectrophotometer (Genesys 10s UV-VIS spectrophotometer, Thermo Fisher Scientific, Waltham, MA, USA) at 664 nm. The results were expressed as average ± standard deviation (S.D.) from three separated experiments.

To measure experimental drug contents, 5 mg of bCDsu-ss-Ce6 nanophotosensitizers were reconstituted in 20 mL PBS with 20 mM GSH and then incubated at 37 ◦C for one day with shaking incubator (100 rpm). This solution was diluted with DMSO more than 10 times and then measured with UV spectrophotometer. Drug contents = [(Ce6 weight/nanophotosensitizer weight) × 100. For comparison, similar weight of bCDsu-ss and GSH were used as blank.

4.7. Cell Culture Study

Cells: CCD986sk human skin fibroblast cells and HeLa human cervical cancer cells were obtained from Korean Cell Line Bank, Co. (Seoul, Korea). CCD986sk cells were cultured using IMDM (Gibco, Grand Island, NY, USA) medium supplemented with 10% heat-inactivated fetal bovine serum (FBS) (Invitrogen) and 1% penicillin/streptomycin. HeLa cells were cultured using MEM (Gibco, Grand Island, NY, USA) medium supplemented with 10% heat-inactivated fetal bovine serum (FBS) (Invitrogen) and 1% penicillin/streptomycin. All cell lines were maintained at 37 ◦C in a 5% CO_2 incubator.

Intracellular Ce6 uptake: HeLa cells seeded into 96-well plates (2×10^4 cells/well) were exposed to Ce6 or bCDsu-ss-Ce6 nanophotosensitizers and, 2 h later, cells were washed with PBS twice. For Ce6 treatment, Ce6 dissolved in DMSO (1 mg Ce6/mL DMSO) was diluted with serum-free media more than 200 times (DMSO final concentration: 0.5% (v/v)) to make 5 μg/mL of Ce6 concentration and then diluted with serum-free media as an appropriate concentration. The nanophotosensitizers in deionized water were filtered with a syringe filter (1.2 μm) and then diluted with serum-free media more than 10 times. Cells were lysed with 50 μL of lysis buffer (GenDEPOT, Barker, TX, USA) to analyze Ce6 contents in the cells. The intracellular Ce6 uptake ratio was analyzed with the relative fluorescence intensity with an Infinite M200pro microplate reader (Tecan) (excitation wavelength: 407 nm, emission wavelength: 664 nm).

Fluorescence microscopy was used to observe cell morphology. Cells seeded on the cover glass in six-well plates (2×10^5 cells/well) were treated with Ce6 or bCDsu-ss-Ce6 nanophotosensitizers (As a Ce6 concentration, 2 μg/mL). After 1 h, cells were washed with PBS twice and then cells were fixed with 4% paraformaldehyde (PFA) solution in PBS for 15 m. These were immobilized with immobilization solution (Immunomount, Thermo Electron Co. Pittsburgh, PA, USA) and observed with a fluorescence microscope (Eclipse 80i; Nikon, Tokyo, Japan).

Flow cytometry analysis of HeLa cells were performed using flow cytometer (NAVIOS, Beckman Coulter Inc., Brea, CA, USA). Cells (2×10^5 cells) were exposed to Ce6 or bCDsu-ss-Ce6 nanophotosensitizers (As a Ce6 concentration, 2 μg/mL). After 1 h, cells were washed with PBS twice and then adopted to measure flow cytometer using Red (635 nm) laser filter at room temperature.

Intracellular ROS generation: The intracellular ROS generation of HeLa cells were analyzed with DCFH-DA. Cells (2×10^4 cells/well) in 96 well plate were exposed to Ce6 or bCDsu-ss-Ce6 nanophotosensitizers in serum-free media and DCFH-DA in PBS was also added (final concentration:

 doi:10.20944/preprints202310.1006.v1

20 μM). After 2 h, cells were washed with PBS twice, replaced with fresh phenol red-free RPMI media (100 μL) and then irradiated at 664 nm (2.0 J/cm^2) using an expanded homogenous beam (SH Systems, Gwangju, Korea). The intracellular ROS was analyzed with a microplate reader (Infinite M200 PRO (Tecan)) (Excitation wavelength, 485 nm; emission wavelength, 535 nm). All procedures were performed in the dark condition.

PDT study against cancer cells: HeLa cells seeded in 96-well plates (2 × 10^4 cells/well) were exposed to Ce6 alone or bCDsu-ss-Ce6 nanophotosensitizers in the Ce6 concentration range of (0.001 ~ 5 μg/mL). The cells were incubated for 2 h in a 5% CO_2 incubator at 37 ◦C and then washed with PBS twice. To these cells, 100 μL of serum-free media were added and then were irradiated at 664 nm (Light dose: 2.0 J/cm^2) using an expanded homogenous beam (SH Systems, Gwangju, Korea). After that, cells were incubated for 24 h in a 5% CO_2 incubator at 37 ◦C. Cell viability was analyzed with MTT assay. MTT solution (30 thirty μL from MTT stock solution (5 mg/mL in PBS)) was added to the 96 wells and then placed into a CO_2 incubator for 4h. After that, supernatants were discarded and then replaced with 100 μL DMSO. The viability of the cells was analyzed by absorbance at 570 nm using an Infinite M200 PRO microplate reader. All procedures for PDT study were carried out in dark conditions.

An intrinsic dark toxicity of CCD986Sk cells and HeLa cells were performed with same procedure in the absence of light irradiation at dark condition.

4.8. Animal Tumor Imaging Using HeLa tumor Xenograft Model In Vivo

For animal study, nude BALb/C mice (male, 20 g, five weeks old, OrientBio Co. Ltd. Seongnamsi, Gyeonggido, Korea) were used. HeLa cells (1 × 10^6 cells) were subcutaneously (s.c.) administered into the backs of nude BALb/C mice. When the diameter of the tumor xenograft became bigger than 6 mm, HeLa cell-bearing mice were used for fluorescence imaging. Aqueous Ce6 solution or nanophotosensitizer solution (10 mg Ce6/kg) was intravenously (i.v.) injected via the tail veins of the mice (injection volume: 200 μL). For Ce6 treatment, Ce6 was dissolved in ethanol/Cremophor EL solution (1/1) and then diluted with PBS more than 10 times. The nanophotosensitizers in deionized water were filtered with a syringe filter (1.2 μm). Maestro™ 2 small animal imaging instrument (Cambridge Research and Instruments, Inc. Woburn, MA, USA) was used to observe fluorescence images of whole bodies of the mice. For imaging of animals, the mice were anesthetized with avertin. For biodistribution of Ce6 or nanophotosensitizers, the organs of mice were extracted. To anesthetize, 0.5 mL of a stock solution of avertin (25 g avertin in 15.5 mL tert-amyl alcohol) was mixed with 39.5 mL of 0.9% saline solution. The avertin solution (300~400 μL/mice) was intraperitoneally (i.p.) administered to anesthetize the mice.

4.9. PDT of HeLa Tumor Xenograft Model In Vivo

PDT of the mice was performed as follows: HeLa cells (1 × 10^6 cells) were subcutaneously (s.c.) administered into the backs of nude BALb/C mice and the mice were divided into three groups: control group, Ce6 treatment group and nanophotosensitizer treatment group. Each group is composed of 5 mice. When the tumor diameters became about 4 mm, Ce6 alone or nanophotosensitizers were i.v. administered (Injection dose: 10 mg Ce6/kg for each mouse). For the control treatment, PBS was administered. Each treatment was administered intravenously via a tail vein of each mouse. Injection volume was 200 μL. After 2 days of administration, the mice were anesthetized with avertin for PDT (2.0 J/cm^2 , 664 nm). To irradiate tumor xenograft of the mice, mice were covered with fabric material to avoid interference of irradiated light except tumor. The day 0 was determined the day of the first irradiation. Three days later, the mice were irradiated once more. The growth of tumor volume was measured with vernier calipers at 5-day intervals. The tumor volume was calculated as follows: tumor volume (mm^3) = (length × width^2)/2.

Animal experiments were carefully performed under the guidelines of the Pusan National University Institutional Animal Care and Use Committee (PNUIACUC). The protocols of this study were reviewed and monitored by the PNUIACUC in accordance with their ethical procedures and scientific care (approval number: PNU-2020-2751).

 doi:10.20944/preprints202310.1006.v1

4.10. Statistical Analysis

The statistical significance was estimated with Student's t-test using SigmaPlot® (SigmaPlot® v.11.0, Systat Software, Inc., San Jose, CA, USA). The minimal level of significance was evaluated as $p < 0.05$.

5. Conclusions

bCDsu-ss-Ce6 conjugates were synthesized for redox-sensitive delivery of photosensitizer, Ce6, and PDT efficacy against HeLa. bCD was succinylated to endow carboxyl groups in bCD (bCDsu) and then Ce6 was conjugated with bCDsu via disulfide linkage (bCDsu-ss-Ce6). Chemical composition of bCDsu-ss-Ce6 was confirmed with ^{1}H and ^{13}C NMR spectra, indicating that Ce6 was conjugated with bCDsu via disulfide linkage. bCDsu-ss-Ce6 conjugates formed nano-scale particles in the aqueous solution, i.e. bCDsu-ss-Ce6 nanophotosensitizers have small particles less than 200 nm with average particle size of 152.0±23.2 nm. They showed improved SO generation in the aqueous solution under light irradiation and SO generation was significantly higher than that of Ce6 alone. Ce6 release rate from bCDsu-ss-Ce6 nanophotosensitizers was accelerated according to the GSH concentration, indicating that bCDsu-ss-Ce6 nanophotosensitizers have redox-sensitive drug release properties. bCDsu-ss-Ce6 nanophotosensitizers have low intrinsic cytotoxicity against CCD986Sk cells as well as Ce6 alone. bCDsu-ss-Ce6 nanophotosensitizers showed enhanced Ce6 uptake ratio, higher ROS production and improved phototoxicity compared to those of Ce6 alone. Furthermore, bCDsu-ss-Ce6 nanophotosensitizers showed higher Ce6 uptake ratio, ROS generation and phototoxicity against HeLa cells in the presence of GSH, indicating that bCDsu-ss-Ce6 nanophotosensitizers have redox-sensitive biological activity in vitro cell culture system. bCDsu-ss-Ce6 nanophotosensitizers efficiently accumulated in the tumor tissue, i.e. their fluorescence intensity was significantly higher in tumor tissues than those of other organs compared to Ce6 alone. These results induced higher anticancer activity of bCDsu-ss-Ce6 nanophotosensitizers, i.e. they efficiently inhibited growth of tumor in vivo animal tumor xenograft study.

Supplementary Materials: The following supporting information can be downloaded at: www.mdpi.com/xxx/s1, Figure S1: (a) ^{1}H and (b) ^{13}C NMR spectra of Ce6. Figure S2. (a) ^{1}H and (b) ^{13}C NMR spectra of bCDsu. Figure S3. Heteronuclear single quantum coherence (HSQC) and heteronuclear multiple bond correlation (HMBC) of bCDsu. Figure S4. (a) ^{1}H and (b) ^{13}C NMR spectra of bCDsu-ss. Figure S5. HSQC and HMBC of bCDsu-ss.

Author Contributions: Conceptualization, Y.-J.L. and Y.-I.J.; methodology, J.J., J.Y.K. and J.-J.Y; validation, Y.-I.J. and Y.-J.L.; formal analysis, J.J., J.Y.K. and J.-J.Y; investigation, J.J., Y.-J.L. and Y.-I.J.; data curation, J.J. and J.Y.K.; writing—original draft preparation, J.J. and Y.-J.L.; writing—review and editing, Y.-I.J.; visualization, Y-.J.L. and Y.-I.J.; supervision, Y.-I.J.; project administration, Y-.J.L.; funding acquisition, Y-.J.L. All authors have read and agreed to the published version of the manuscript.

Funding: This work was supported by grants from the Korea Basic Science Institute (grant number C330340) and the Support for Return to R&D program (WISET) (grant number PG2022133).

Institutional Review Board Statement: Animal experiments were carefully performed under the guidelines of the Pusan National University Institutional Animal Care and Use Committee (PNUIACUC). The protocols of this study were reviewed and monitored by the PNUIACUC in accordance with their ethical procedures and scientific care (approval number: PNU-2020-2751).

Informed Consent Statement: Not applicable.

Data Availability Statement: Not applicable.

Acknowledgments: In this section, you can acknowledge any support given which is not covered by the author contribution or funding sections. This may include administrative and technical support, or donations in kind (e.g., materials used for experiments).

Conflicts of Interest: The authors declare no conflict of interest.

References

1. Yanovsky, R.L.; Bartenstein, D.W.; Rogers, G.S.; Isakoff, S.J.; Chen, S.T. Photodynamic therapy for solid tumors: A review of the literature. *Photodermatol. Photoimmunol. Photomed*. **2019**, *35*, 295–303.
2. Pass, H.I. Photodynamic therapy in oncology: mechanisms and clinical use. *J. Natl. Cancer Inst*. **1993**, *85(6)*, 443–456.
3. Kawczyk-Krupka, A.; Bugaj, A.M.; Latos, W.; Zaremba, K.; Wawrzyniec, K.; Siero ´n, A. Photodynamic therapy in colorectal cancer treatment: The state of the art in clinical trials. *Photodiagn. Photodyn. Ther*. **2015**, *12*, 545–553.
4. Kato, H.; Furukawa, K.; Sato, M.; Okunaka, T.; Kusunoki, Y.; Kawahara, M.; Fukuoka, M.; Miyazawa, T.; Yana, T.; Matsui, K.; et al. Phase II clinical study of photodynamic therapy using mono-L-aspartyl chlorin e6 and diode laser for early superficial squamous cell carcinoma of the lung. *Lung Cancer* **2003**, *42*, 103–111.
5. Scherer, K.M.; Bisby, R.H.; Botchway, S.W.; Parker, A.W. New approaches to photodynamic therapy from types I, II and III to type IV using one or more photons. *Anticancer Agents Med. Chem*. **2017**, *17*, 171–189.
6. Mallidi, S.; Anbil, S.; Bulin, A.L.; Obaid, G.; Ichikawa, M.; Hasan, T. Beyond the barriers of light penetration: Strategies, per-spectives and possibilities for photodynamic therapy. Theranostics **2016**, *6*, 2458–2487.
7. Inglut, C.T.; Gaitan, B.; Najafali, D.; Lopez, I.A.; Connolly, N.P.; Orsila, S.; Perttilä, R.; Woodworth, G.F.; Chen, Y.; Huang, H.C. Predictors and limitations of the penetration depth of photodynamic effects in the rodent brain. *Photochem. Photobiol*. **2020**, *96*, 301–309.
8. Stringasci, M.D.; Fortunato, T.C.; Moriyama, L.T.; Filho, J.D.V.; Bagnato, V.S.; Kurachi, C. Interstitial PDT using diffuser fiber investigation in phantom and in vivo models. *Lasers Med. Sci*. **2017**, *32*, 1009–1016.
9. Bosch, F.X.; de Sanjosé, S. The epidemiology of human papillomavirus infection and cervical cancer. Dis. Markers 2007, 23, 213–227.
10. Rallis, K.S.; Lai Yau, T.H.; Sideris, M. Chemoradiotherapy in cancer treatment: Rationale and clinical applications. *Anticancer Res*. **2021**, *41*, 1–7.
11. Peng, Q.; Warloe, T.; Berg, K.; Moan, J.; Kongshaug, M.; Giercksky, K.E.; Nesland, J.M. 5-Aminolevulinic acid-based photodynamic therapy. Clinical research and future challenges. *Cancer*. **1997**, *79(12)*, 2282-2308.
12. Popken, G.; Schultze-Seemann, W.; Seiler, K.U.; Birkel, M.; Wetterauer, U. Intravesical administration of 5-aminolevulinic acid (5-ALA). Safety and pharmacokinetics of 5-ALA and its metabolite protoporphyrin IX. *Eur. J. Clin. Pharmacol*. **2000**, *56*, 241-246.
13. Bissonnette, R.; Nigen, S.; Bolduc, C.; Méry, S.; Nocera, T. Protection afforded by sunscreens containing inorganic sunscreening agents against blue light sensitivity induced by aminolevulinic acid. *Dermatol. Surg*. **2008**, *34*, 1469-1476.
14. Rosin, F.C.P.; Teixeira, M.G.; Pelissari, C.; Corrêa, L. Resistance of oral cancer cells to 5-ALA-mediated photodynamic therapy. *J. Cell Biochem*. **2018**, *119*, 3554-3562.
15. Rosin, F.C.P.; Teixeira, M.G.; Pelissari, C.; Corrêa, L. Photodynamic therapy mediated by 5-aminolevulinic acid promotes the upregulation and modifies the intracellular expression of surveillance proteins in oral squamous cell carcinoma. *Photochem. Photobiol*. **2019**, *95*, 635-643.
16. Lin, B.; Xu, X.; Zhang, X.; Yu, Y.; Wang, X. Photodynamic treatment of colorectal cancer using chlorin e6-loaded poly(lactide-co-glycolide)-based nanoparticles. *J. Biomed. Nanotechnol*. **2021**, *17*, 1939-1950.
17. Huang, L.; Zhiyentayev, T.; Xuan, Y.; Azhibek, D.; Kharkwal, G.B.; Hamblin, M.R. Photodynamic inactivation of bacteria using polyethylenimine-chlorin(e6) conjugates: Effect of polymer molecular weight, substitution ratio of chlorin(e6) and pH. *Lasers Surg. Med*. **2011**, *43*, 313-323.
18. Zhang, X.; Feng, L.; Dong, Z.; Xin, X.; Yang, Z.; Deng, D.; Wagner, E.; Liu, Z.; Liu, X. Protein-drug conjugate programmed by pH-reversible linker for tumor hypoxia relief and enhanced cancer combination therapy. *Int. J. Pharm*. **2020**, *582*, 119321.
19. Castilho, M.L.; Jesus, V.P.S.; Vieira, P.F.A.; Hewitt, K.C.; Raniero, L. Chlorin e6-EGF conjugated gold nanoparticles as a nanomedicine based therapeutic agent for triple negative breast cancer. *Photodiagnosis Photodyn. Ther*. **2021**, *33*, 102186.
20. Paul, S.; Heng, P.W.; Chan, L.W. pH-dependent complexation of hydroxypropyl-beta-cyclodextrin with chlorin e6: effect on solubility and aggregation in relation to photodynamic efficacy. *J. Pharm. Pharmacol*. **2016**, *68(4)*, 439-449.
21. Mitchell, M.J.; Billingsley, M.M.; Haley, R.M.; Wechsler, M.E.; Peppas, N.A.; Langer, R. Engineering precision nanoparticles for drug delivery. *Nat. Rev. Drug Discov*. **2021**, *20*, 101-124.
22. Hwang, D.; Ramsey, J.D.; Kabanov, A.V. Polymeric micelles for the delivery of poorly soluble drugs: From nanoformulation to clinical approval. *Adv. Drug Deliv. Rev*. **2020**, *156*, 80-118.
23. Zhou, Q.; Zhang, L.; Yang, T.; Wu, H. Stimuli-responsive polymeric micelles for drug delivery and cancer therapy. *Int. J Nanomedicine*. **2018**, *13*, 2921-2942.

24. Li, J.; Liu, S.; Gao, Y.; Li, Z.; Cai, J.; Zhang, Q.; Li, K.; Liu, Z.; Shi, M.; Wang, J.; Li, Q. Layered and orthogonal assembly of hydrophilic drugs and hydrophobic photosensitizers for enhanced cancer therapy. *Biomater. Adv*. **2022**,*133*, 112598.
25. Wang, T.; Zhang, H.; Han, Y.; Liu, H.; Ren, F.; Zeng, J.; Sun, Q.; Li, Z.; Gao, M. Light-enhanced O_2-evolving nanoparticles boost photodynamic therapy to elicit antitumor immunity. *ACS Appl Mater Interfaces*. **2019**, *11*, 16367-16379.
26. Xue, E.Y.; Shi, W.J.; Fong, W.P.; Ng, D.K.P. Targeted delivery and site-specific activation of β-cyclodextrin-conjugated photosensitizers for photodynamic therapy through a supramolecular bio-orthogonal approach. *J. Med. Chem*. **2021**, *64*, 15461-15476.
27. Bansal, A.; Simon, M.C. Glutathione metabolism in cancer progression and treatment resistance. *J. Cell Biol*. **2018**, *217*, 2291–2298.
28. Amreddy, N.; Babu, A.; Muralidharan, R.; Panneerselvam, J.; Srivastava, A.; Ahmed, R.; Mehta, M.; Munshi, A.; Ramesh, R. Recent advances in nanoparticle-based cancer drug and gene delivery. *Adv. Cancer Res*. **2018**, *137*, 115-170.
29. Ghosh, B.; Biswas, S. Polymeric micelles in cancer therapy: State of the art. *J. Control. Release*. **2021**, *332*, 127-147.
30. Modi, S.; Prakash Jain, J.; Domb, A.J.; Kumar, N. Exploiting EPR in polymer drug conjugate delivery for tumor targeting. *Curr. Pharm. Des*. **2006**, *12*, 4785-4796.
31. Cheng, Z.; Li, M.; Dey, R.; Chen, Y. Nanomaterials for cancer therapy: current progress and perspectives. *J. Hematol. Oncol*. **2021**, *14*, 85.
32. Ogawara, K.; Yoshizawa, Y.; Un, K.; Araki, T.; Kimura, T.; Higaki, K. Nanoparticle-based passive drug targeting to tumors: considerations and implications for optimization. *Biol. Pharm. Bull*. **2013**, *36*, 698-702.
33. Liu, Y.; Li, K.; Liu, B.; Feng, S.S. A strategy for precision engineering of nanoparticles of biodegradable copolymers for quantitative control of targeted drug delivery. *Biomaterials*. **2010**, *31*, 9145-9155.
34. Mitchell, M.J.; Billingsley, M.M.; Haley, R.M.; Wechsler, M.E.; Peppas, N.A.; Langer, R. Engineering precision nanoparticles for drug delivery. *Nat. Rev. Drug Discov*. **2021**, *20*, 101-124.
35. Gao, Q.; Huang, D.; Deng, Y.; Yu, W.; Jin, Q.; Ji, J.; Fu, G. Chlorin e6 (Ce6)-loaded supramolecular polypeptide micelles with enhanced photodynamic therapy effect against Pseudomonas aeruginosa. *Chem. Eng. J*. **2021**, *417*, 129334.
36. Sánchez-Iglesias, A.; Grzelczak, M.; Altantzis, T.; Goris, B.; Pérez-Juste, J.; Bals, S.; Van Tendeloo, G.; Donaldson, S.H. Jr; Chmelka, B.F.; Israelachvili, J.N.; Liz-Marzán, L.M. Hydrophobic interactions modulate self-assembly of nanoparticles. *ACS Nano*. **2012**, *6*, 11059-11065.
37. Jeong, Y.I.; Cheon, J.B.; Kim, S.H.; Nah, J.W.; Lee, Y.M.; Sung, Y.K.; Akaike, T.; Cho, C.S. Clonazepam release from core-shell type nanoparticles in vitro. *J. Control. Release*. **1998**, *51*, 169-178.
38. Gu, A.; Wheate, N.J. Macrocycles as drug-enhancing excipients in pharmaceutical formulations. *J. Incl. Phenom. Macrocycl. Chem.* **2021**, *100*, 55–69.
39. Uekama, K.; Hirayama, F.; Irie, T. Cyclodextrin drug carrier systems. *Chem. Rev*. **1998**, *98(5)*, 2045-2076.
40. Sheng, T.M.; Kumar, P.V. A new approach for β-cyclodextrin conjugated drug delivery system in cancer therapy. *Curr. Drug Deliv*. **2022**, *19*, 266-300.
41. Becket, G.; Schep, L.J.; Tan, M.Y. Improvement of the in vitro dissolution of praziquantel by complexation with alpha-, beta- and gamma-cyclodextrins. *Int. J. Pharm*. **1999**, *179*, 65-71.
42. Paul, S.; Heng, P.W.; Chan, L.W. pH-dependent complexation of hydroxypropyl-beta-cyclodextrin with chlorin e6: effect on solubility and aggregation in relation to photodynamic efficacy. *J. Pharm. Pharmacol*. **2016**, *68*, 439-449.
43. Li, J.; Liu, S.; Gao, Y.; Li, Z.; Cai, J.; Zhang, Q.; Li, K.; Liu, Z.; Shi, M.; Wang, J.; Li, Q. Layered and orthogonal assembly of hydrophilic drugs and hydrophobic photosensitizers for enhanced cancer therapy. *Biomater. Adv*. **2022**, *133*, 112598.
44. Behzadi, S.; Serpooshan, V.; Tao, W.; Hamaly, M.A.; Alkawareek, M.Y.; Dreaden, E.C.; Brown, D.; Alkilany, A.M.; Farokhzad, O.C.; Mahmoudi, M. Cellular uptake of nanoparticles: journey inside the cell. *Chem. Soc. Rev*. **2017**, *46*, 4218-4244.
45. Thakur, N.S.; Mandal, N.; Patel, G.; Kirar, S.; Reddy, Y.N.; Kushwah, V.; Jain, S.; Kalia, Y.N.; Bhaumik, J.; Banerjee, U.C. Co-administration of zinc phthalocyanine and quercetin via hybrid nanoparticles for augmented photodynamic therapy. *Nanomedicine*. **2021**, *33*, 102368.
46. Hirsjärvi, S.; Passirani, C.; Benoit, J.P. Passive and active tumor targeting with nanocarriers. *Curr. Drug Discov. Technol*. **2011**, *8*, 188–196.
47. Danhier, F.; Feron, O.; Préat, V. To exploit the tumor microenvironment: Passive and active tumor targeting of nanocarriers for anti-cancer drug delivery. *J. Control. Release* **2010**, *148*, 135–146.

48. Dai, Y.; Xu, C.; Sun, X.; Chen, X. Nanoparticle design strategies for enhanced anticancer therapy by exploiting the tumor microenvironment. *Chem. Soc. Rev*. **2017**, *46*, 3830–3852.
49. Sosa, V.; Moliné, T.; Somoza, R.; Paciucci, R.; Kondoh, H.; LLeonart, M.E. Oxidative stress and cancer: An overview. *Ageing Res. Rev*. **2013**, *12*, 376–390.
50. Welters, M.J.; Fichtinger-Schepman, A.M.; Baan, R.A.; Flens, M.J.; Scheper, R.J.; Braakhuis, B.J. Role of glutathione, glutathione S-transferases and multidrug resistance-related proteins in cisplatin sensitivity of head and neck cancer cell lines. *Br. J. Cancer* **1998**, *77(4)*, 556–561.
51. Nunes, S.C.; Serpa, J. Glutathione in ovarian cancer: A double-edged sword. *Int. J. Mol. Sci.* **2018**, *19*, 1882.
52. Parkhats, M.V.; Galievskii, V.A.; Zharnikova, E.S.; Knyukshto, V.N.; Lepeshkevich, S.V.; Stashevskii, A.S.; Trukhacheva, T.V.; Dzhagarov, B. M. Dynamics of photosensitized singlet oxygen generation and photophysical characteristics of chlorin e_6 in photolon ointment. *J. Appl. Spectrosc.* **2011**, *78*, 278–285.
53. Lee, H.M.; Chung, C.W.; Kim, C.H.; Kim, D.H.; Kwak, T.W.; Jeong, Y.I.; Kang, D.H. Defensive mechanism in cholangiocarcinoma cells against oxidative stress induced by chlorin e6-based photodynamic therapy. *Drug Des. Devel. Ther*. **2014**, *8*, 1451-62.
54. García, A..; Leonardi, D.; Lamas, M. Promising applications in drug delivery systems of a novel β-cyclodextrin derivative obtained by green synthesis. *Bioorg. Med. Chem. Lett*. **2016**, *26*, 602-608.